

Rotating star initial data for a constrained scheme in numerical relativity

Lap-Ming Lin and Jérôme Novak

Laboratoire de l'Univers et de ses Théories, Observatoire de Paris, F-92195
Meudon Cedex, France

Abstract. A new numerical code for computing stationary axisymmetric rapidly rotating stars in general relativity is presented. The formulation is based on a fully constrained-evolution scheme for $3 + 1$ numerical relativity using the Dirac gauge and maximal slicing. We use both the polytropic and MIT bag model equations of state to demonstrate that the code can construct rapidly rotating neutron star and strange star models. We compare numerical models obtained by our code and a well-established code, which uses a different gauge condition, and show that the two codes agree to high accuracy.

PACS numbers: 04.25.Dm, 04.40.Dg

1. Introduction

In the $3 + 1$ formalism of general relativity, the Einstein equations are decomposed into a set of four constraint equations and six evolution equations [1, 2]. Solving the (elliptic-type) constraint equations at each time-step in multidimensional simulations is in general not feasible as it is computationally expensive for most numerical techniques. Hence, a free-evolution approach, i.e., solving the constraint equations only for the initial data and performing the evolutions without enforcing the constraints, is generally favoured over a fully constrained scheme (solving the constraints at each time step) in three-dimensional numerical simulations. While mathematically the constraints are preserved by the evolution equations, in practice small constraint violations due to numerical errors typically grow quickly to a significant level that make the solution unphysical and plague the simulations. Although numerous techniques to control the growth of constraint violations have been developed (e.g., [3, 4, 5, 6, 7, 8]), it is not clear yet to what extent they can control the constraint violations successfully in general.

Fully constrained-evolution scheme has been used in the past only in spherically symmetric or axisymmetric problems (e.g., [9, 10, 11, 12]). The main advantage of a fully constrained scheme is that the constraints are fulfilled to within the discretisation errors, and the constraint-violating modes do not exist by construction. Recently, a new formulation for $3 + 1$ numerical relativity based on a fully constrained-evolution scheme is proposed by Bonazzola *et al.* [13]. The chosen coordinate conditions (maximal slicing and Dirac gauge, see Sec. 2.3), together with the use of spherical components of tensor fields, reduce the ten Einstein equations to a system of five quasi-linear elliptic equations, which are solved by efficient multi-domain spectral methods, and two quasi-linear scalar wave equations [13]. The Dirac gauge is used to fix the

remaining three degrees of freedom. The stability of the proposed scheme has been demonstrated for a three-dimensional pure gravitational wave spacetime [13].

In the proposed constrained scheme, the coordinates are fixed by the Dirac gauge on each hypersurface (with maximal slicing condition), including the initial one. This implies that initial data must be prepared in the same coordinate choices in order to perform dynamical evolutions. As an advantage of this gauge-fixing, stationary solutions of the Einstein equations can be computed within the same framework simply by setting the time derivative terms to zero in the equations. The aim of the present work is to construct rotating-star initial data for this new formulation of 3 + 1 numerical relativity. For this purpose, we have developed a numerical code to calculate stationary axisymmetric rotating star models based on the Dirac gauge and maximal slicing.

The purpose of this paper is to present the formulation of the problem and the tests that have been done to validate our numerical code. The numerical code can be used to provide initial rotating star models for hydrodynamics simulations in full general relativity within the new formulation. Our emphasis here is put on the comparison of the accuracy between our code and a well-established code LORENE-rotstar [14, 15, 16]. In particular, we demonstrate that our numerical code can compute rapidly rotating neutron star and strange star models to high accuracy. Unless otherwise noted, we use units such that $G = c = 1$. Latin (Greek) indices go from 1 to 3 (0 to 3).

2. Formulation

2.1. The 3 + 1 decomposition

In this section, we give a brief description of the 3 + 1 formulation of the Einstein equations in order to define our notations (see, e.g., [1, 2] for details). In the 3 + 1 formalism, the spacetime is foliated by a family of spacelike hypersurfaces Σ_t , labelled by the time coordinate t . Introducing a coordinate system (x^i) on each hypersurface, the line element may be written as

$$ds^2 = -N^2 dt^2 + \gamma_{ij}(dx^i + \beta^i dt)(dx^j + \beta^j dt), \quad (1)$$

where N is the lapse function, β^i is the shift vector, and γ_{ij} is the 3-metric induced by the spacetime metric $g_{\alpha\beta}$ onto each hypersurface Σ_t

$$\gamma_{\alpha\beta} := g_{\alpha\beta} + n_\alpha n_\beta. \quad (2)$$

Here $n_\alpha := -N\nabla_\alpha t$ is the unit normal to Σ_t , where ∇_α is the covariant derivative associated with the spacetime metric $g_{\alpha\beta}$. The stress-energy tensor $T^{\alpha\beta}$ is decomposed as

$$T^{\alpha\beta} = E n^\alpha n^\beta + n^\alpha J^\beta + J^\alpha n^\beta + S^{\alpha\beta}, \quad (3)$$

where $E := T_{\alpha\beta} n^\alpha n^\beta$, $J_\alpha := -\gamma_\alpha^\mu T_{\mu\nu} n^\nu$, and $S_{\alpha\beta} := \gamma_\alpha^\mu \gamma_\beta^\nu T_{\mu\nu}$ are the energy density, momentum density, and the stress tensor, as measured by the observers of 4-velocity n^α (the so-called Eulerian observers O_e).

The evolution of the 3-metric γ_{ij} is governed by

$$\frac{\partial}{\partial t} \gamma_{ij} - \mathcal{L}_\beta \gamma_{ij} = -2N K_{ij}, \quad (4)$$

where \mathcal{L} is the Lie derivative operator and K_{ij} is the extrinsic curvature of Σ_t . The evolution equation for K_{ij} is

$$\begin{aligned} \frac{\partial}{\partial t} K_{ij} - \mathcal{L}_\beta K_{ij} = & - D_i D_j N + N \{ R_{ij} - 2K_{ij} K^{ij} + K K_{ij} \\ & + 4\pi[(S - E)\gamma_{ij} - 2S_{ij}]\}, \end{aligned} \quad (5)$$

where D_i is the covariant derivative associated with the 3-metric γ_{ij} , R_{ij} is the Ricci tensor associated with this 3-metric, $K := K^i_i$ is the trace of the extrinsic curvature, and $S := S^i_i$. In the 3+1 formulation, the full set of Einstein equations is equivalent to the above evolution equations, together with the Hamiltonian constraint

$$R + K^2 - K_{ij} K^{ij} = 16\pi E, \quad (6)$$

and the momentum constraint

$$D_j K_i^j - D_i K = 8\pi J_i, \quad (7)$$

where $R := R^i_i$ is the three-dimensional Ricci scalar.

2.2. The matter sources: uniformly rotating fluid

We assume that the matter consists of a perfect fluid with a stress-energy tensor

$$T^{\alpha\beta} = (e + P)u^\alpha u^\beta + P g^{\alpha\beta}, \quad (8)$$

where u^α is the 4-velocity of the fluid; e and P are respectively the energy density and pressure, as measured by the the fluid comoving observer O_f . Defining the Lorentz factor linking the two observers O_e and O_f by

$$\Gamma := -n_\alpha u^\alpha = N u^t, \quad (9)$$

the energy density E in Eq. (3) can be written as

$$E = \Gamma^2(e + P) - P. \quad (10)$$

The momentum density J^i is

$$J^i = (E + P)v^i, \quad (11)$$

where the fluid 3-velocity v^i is related to the spatial components of the fluid 4-velocity u^i by

$$u^i = \Gamma \left(v^i - \frac{\beta^i}{N} \right). \quad (12)$$

Note that the Lorentz factor can be expressed as $\Gamma = (1 - v^2)^{-1/2}$, where $v := (v_i v^i)^{1/2}$ is the “physical” fluid speed as measured by the Eulerian observer O_e . The stress tensor S_{ij} is given by

$$S_{ij} = (E + P)v_i v_j + P\gamma_{ij}. \quad (13)$$

Up to this point, we have not made any assumptions on the spacetime and fluid flow. Now consider that the spacetime is stationary, axisymmetric, and asymptotically flat. These assumptions imply the existence of two Killing vector fields: $\vec{\zeta}$, which is timelike at spatial infinity; $\vec{\chi}$, which is spacelike everywhere and with closed orbits. Furthermore, the Killing vectors commute [17], and hence we can choose an adapted coordinate system (t, x^1, x^2, φ) , such that $\vec{\zeta} = \partial/\partial t$ and $\vec{\chi} = \partial/\partial\varphi$ are the coordinate vector fields (see also [14]). We choose the remaining two coordinates to be of spherical

type (i.e., $x^1 = r$ and $x^2 = \theta$). Next we assume that the fluid is purely axial (i.e., no meridional convective currents), for which the fluid 4-velocity is given by

$$\vec{u} = u^t \left(\frac{\partial}{\partial t} + \Omega \frac{\partial}{\partial \varphi} \right), \quad (14)$$

where $\Omega := u^\varphi/u^t$ is the fluid coordinate angular velocity, and can be interpreted as the fluid angular velocity as seen by an inertial observer at rest at infinity.

The equation of stationary motion follows from the projection of the conservation equation $\nabla_\alpha T^{\alpha\beta} = 0$ normal to the 4-velocity u^α . In this paper, we focus on the case of uniformly rotating star (i.e., Ω is a constant). Together with the assumption that the fluid is barotropic, the first integral of motion can be written as (see, e.g., [14])

$$H + \ln N - \ln \Gamma = \text{const.}, \quad (15)$$

where H is the log-enthalpy defined by

$$H := \int \frac{dP}{e + P}. \quad (16)$$

2.3. The metric equations

Here we summarise the full set of Einstein equations in the constrained-evolution scheme based on the Dirac gauge and maximal slicing. We refer the reader to Ref. [13] for details and derivations. First, we define a conformal metric $\tilde{\gamma}_{ij}$ by

$$\tilde{\gamma}_{ij} := \Psi^{-4} \gamma_{ij}, \quad (17)$$

with the conformal factor Ψ defined by

$$\Psi := \left(\frac{\det \gamma_{ij}}{\det f_{ij}} \right)^{1/12}, \quad (18)$$

where f_{ij} is a flat 3-metric, given by the asymptotic condition on γ_{ij} . The four constraint equations (6) and (7), together with the maximal slicing condition $K = 0$, result in two scalar equations for the lapse and conformal factor; and one vectorial elliptic equations for the shift vector.

The lapse function N is given by

$$\Delta N = \Psi^4 N \left[4\pi(E + S) + \tilde{A}_{kl} A^{kl} \right] - h^{kl} \mathcal{D}_k \mathcal{D}_l N - 2\tilde{D}_k \Phi \tilde{D}^k N, \quad (19)$$

where \mathcal{D}_i is the covariant derivative associated with the flat metric f_{ij} and its contravariant component is defined by $\mathcal{D}^i := f^{ij} \mathcal{D}_j$; $\Delta := f^{ij} \mathcal{D}_i \mathcal{D}_j$ is the flat-space Laplacian operator; \tilde{D}_i is the covariant derivative associated with the conformal metric $\tilde{\gamma}_{ij}$ and its contravariant component is $\tilde{D}^i := \tilde{\gamma}^{ij} \tilde{D}_j$ (with the inverse conformal metric $\tilde{\gamma}^{ij}$ defined by $\tilde{\gamma}_{ik} \tilde{\gamma}^{kj} = \delta_i^j$). The quantity Φ is defined by $\Phi := \ln \Psi$. The traceless part of the conformal extrinsic curvature A^{ij} is defined by

$$A^{ij} := \Psi^4 \left(K^{ij} - \frac{1}{3} \gamma^{ij} K \right), \quad (20)$$

while the tensor field \tilde{A}_{ij} is defined by

$$\tilde{A}_{ij} := \tilde{\gamma}_{ik} \tilde{\gamma}_{jl} A^{kl} = \Psi^{-4} \left(K_{ij} - \frac{1}{3} \gamma_{ij} K \right). \quad (21)$$

The tensor field h^{ij} on the right-hand side (RHS) of Eq. (19) is the deviation of the inverse conformal metric from the inverse flat metric defined by

$$h^{ij} := \tilde{\gamma}^{ij} - f^{ij}. \quad (22)$$

In the proposed constrained scheme, the Dirac gauge condition is given by

$$\mathcal{D}_j h^{ij} = 0. \quad (23)$$

Next, the conformal factor Ψ (or equivalently $Q := \Psi^2 N$) is determined from

$$\begin{aligned} \Delta Q = & -h^{kl} \mathcal{D}_k \mathcal{D}_l Q + \Psi^6 \left[N \left(4\pi S + \frac{3}{4} \tilde{A}_{kl} A^{kl} \right) \right] \\ & + 2\Psi^2 \left[N \left(\frac{\tilde{R}_*}{8} + \tilde{D}_k \Phi \tilde{D}^k \Phi \right) + \tilde{D}_k \Phi \tilde{D}^k N \right], \end{aligned} \quad (24)$$

where the quantity \tilde{R}_* on the RHS is given by

$$\tilde{R}_* := \frac{1}{4} \tilde{\gamma}^{kl} \mathcal{D}_k h^{mn} \mathcal{D}_l \tilde{\gamma}_{mn} - \frac{1}{2} \tilde{\gamma}^{kl} \mathcal{D}_k h^{mn} \mathcal{D}_n \tilde{\gamma}_{ml}. \quad (25)$$

The elliptic equation for the shift vector is

$$\begin{aligned} \Delta \beta^i + \frac{1}{3} \mathcal{D}^i (\mathcal{D}_j \beta^j) = & 16\pi N \Psi^4 J^i + 2A^{ij} \mathcal{D}_j N - 12NA^{ij} \mathcal{D}_j \Phi - 2N\Delta^i_{kl} A^{kl} \\ & - h^{kl} \mathcal{D}_k \mathcal{D}_l \beta^i - \frac{1}{3} h^{ik} \mathcal{D}_k \mathcal{D}_l \beta^l, \end{aligned} \quad (26)$$

where the tensor field Δ^k_{ij} is defined by

$$\Delta^k_{ij} := \frac{1}{2} \tilde{\gamma}^{kl} (\mathcal{D}_i \tilde{\gamma}_{lj} + \mathcal{D}_j \tilde{\gamma}_{il} - \mathcal{D}_l \tilde{\gamma}_{ij}). \quad (27)$$

Now we turn to the dynamical part of the Einstein equations. In the proposed constrained scheme, one solves for the tensor field h^{ij} instead of $\tilde{\gamma}^{ij}$. The evolution equation in this formulation is given by a flat-space (second-order) wave equation for h^{ij} (see Eq. (85) of Ref. [13]). As mentioned in Sec. 1, one advantage of using the Dirac gauge to fix the coordinates on each slice Σ_t is that stationary solutions of the Einstein equations can be computed within the same scheme, simply by setting the time-derivative terms to zeros in the equations. This is possible because of the existence of the Killing vector $\vec{\zeta} = \partial/\partial t$ as discussed in Sec. 2.2. This reduces the wave equation for h^{ij} to the following tensorial Poisson-like equation:

$$\begin{aligned} \Delta h^{ij} = & \frac{\Psi^4}{N^2} \left\{ \mathcal{L}_\beta \mathcal{L}_\beta h^{ij} + \frac{4}{3} \mathcal{D}_k \beta^k \mathcal{L}_\beta h^{ij} + \frac{N}{\Psi^6} \mathcal{D}_k Q (\mathcal{D}^i h^{jk} + \mathcal{D}^j h^{ik} - \mathcal{D}^k h^{ij}) - 2N \mathcal{S}^{ij} \right. \\ & \left. - \frac{2}{3} \mathcal{D}_k \beta^k (L\beta)^{ij} + 2(\mathcal{L}_\beta N) A^{ij} + \frac{2}{3} \left[\mathcal{L}_\beta (\mathcal{D}_k \beta^k) + \frac{2}{3} (\mathcal{D}_k \beta^k)^2 \right] h^{ij} \right. \\ & \left. - \mathcal{L}_\beta (L\beta)^{ij} \right\}, \end{aligned} \quad (28)$$

where the notation $(L\beta)^{ij}$ stands for the conformal Killing operator associated with the flat metric acting on the shift vector β^i :

$$(L\beta)^{ij} := \mathcal{D}^i \beta^j + \mathcal{D}^j \beta^i - \frac{2}{3} \mathcal{D}_k \beta^k f^{ij}. \quad (29)$$

The tensor field \mathcal{S}^{ij} on the RHS of Eq. (28) is given by

$$\begin{aligned} \mathcal{S}^{ij} = & \Psi^{-4} \left\{ N \left(\tilde{R}_*^{ij} + 8\tilde{D}^i \Phi \tilde{D}^j \Phi \right) + 4 \left(\tilde{D}^i \Phi \tilde{D}^j N + \tilde{D}^j \Phi \tilde{D}^i N \right) \right. \\ & - \frac{1}{3} \left[N \left(\left[\tilde{R}_* + 8\tilde{D}_k \Phi \tilde{D}^k \Phi \right] \tilde{\gamma}^{ij} \right) + 8\tilde{D}_k \Phi \tilde{D}^k N \tilde{\gamma}^{ij} \right] \left. \right\} \\ & + 2N \left[\tilde{\gamma}_{kl} A^{ik} A^{jl} - 4\pi \left(\Psi^4 S^{ij} - \frac{1}{3} S \tilde{\gamma}^{ij} \right) \right] \\ & - \Psi^{-6} \left[\tilde{\gamma}^{ik} \tilde{\gamma}^{jl} \mathcal{D}_k \mathcal{D}_l Q + \frac{1}{2} \left(h^{ik} \mathcal{D}_k h^{lj} + h^{kj} \mathcal{D}_k h^{il} - h^{kl} \mathcal{D}_k h^{ij} \right) \mathcal{D}_l Q \right. \\ & \left. - \frac{1}{3} \left(\tilde{\gamma}^{kl} \mathcal{D}_k \mathcal{D}_l Q \tilde{\gamma}^{ij} \right) \right], \end{aligned} \quad (30)$$

with

$$\begin{aligned} \tilde{R}_*^{ij} = & \frac{1}{2} \left[h^{kl} \mathcal{D}_k \mathcal{D}_l h^{ij} - \mathcal{D}_l h^{ik} \mathcal{D}_k h^{jl} - \tilde{\gamma}_{kl} \tilde{\gamma}^{mn} \mathcal{D}_m h^{ik} \mathcal{D}_n h^{jl} \right. \\ & \left. + \tilde{\gamma}_{nl} \mathcal{D}_k h^{mn} \left(\tilde{\gamma}^{ik} \mathcal{D}_m h^{jl} + \tilde{\gamma}^{jk} \mathcal{D}_m h^{il} \right) + \frac{1}{2} \tilde{\gamma}^{ik} \tilde{\gamma}^{jl} \mathcal{D}_k h^{mn} \mathcal{D}_l \tilde{\gamma}_{mn} \right]. \end{aligned} \quad (31)$$

Furthermore, after setting the time-derivative term of h^{ij} to zero, the conformal extrinsic curvature A^{ij} as defined in Eq. (20) is deduced from (see Eq. (92) of [13])

$$A^{ij} = \frac{1}{2N} \left[(L\beta)^{ij} - \mathcal{L}_\beta h^{ij} - \frac{2}{3} \mathcal{D}_k \beta^k h^{ij} \right]. \quad (32)$$

In summary, to calculate stationary axisymmetric uniformly rotating star models in the framework of the constrained scheme [13] based on the Dirac gauge and maximal slicing, one needs to solve for two scalar elliptic equations (19) and (24) respectively for N and Ψ , a vectorial Poisson-like equation (26) for β^i , and a tensorial elliptic equation (28) for h^{ij} , together with the first integral of motion Eq. (15) for the matter. The numerical procedure on how to solve this system of equations is described in Sec. 3.1.

2.4. Global quantities

We list here various global quantities relevant to axisymmetric rotating-star spacetimes. These gauge invariant quantities are useful to estimate the accuracy of our numerical code as they provide a direct comparison between our code and a different code, which uses a different gauge condition, as presented in Sec. 3.3.

Given a baryon current nu^α , where n is the number density in the fluid frame, the baryon mass of the star is expressed as

$$M_b = m_B \int [-n_\alpha (nu^\alpha)] dV = m_B \int \Gamma n dV, \quad (33)$$

where m_B is the baryon rest mass, $dV = \sqrt{\gamma} d^3x$ is the proper 3-volume element (with γ being the determinant of the 3-metric), and we have used Eq. (9) in the second equality. As we follow Ref. [13] to expand all tensor fields onto the spherical basis $(\mathbf{e}_i) = (\frac{\partial}{\partial r}, \frac{1}{r} \frac{\partial}{\partial \theta}, \frac{1}{r \sin \theta} \frac{\partial}{\partial \varphi})$, which is orthonormal with respect to the flat metric, the proper volume element is written explicitly as $dV = \sqrt{\gamma} r^2 \sin \theta dr d\theta d\varphi$. Notice that we denote by $\hat{\gamma}$ the determinant of the 3-metric expanded onto the basis (\mathbf{e}_i) . Here and afterward we denote by $(\hat{r}, \hat{\theta}, \hat{\varphi})$ indices of specific components on the orthonormal basis (\mathbf{e}_i) .

The gravitational mass M_g is given by the Komar integral (see Eq. (11.2.10) of [18])

$$M_g = 2 \int \left(T_{\alpha\beta} - \frac{1}{2} T g_{\alpha\beta} \right) n^\alpha \zeta^\beta dV, \quad (34)$$

where $T := T^\alpha_\alpha$ and ζ^α is the timelike Killing vector discussed in Sec. 2.2. Explicitly, we have

$$M_g = \int [N(E + S) - 2J_{\hat{\varphi}}\beta^{\hat{\varphi}}] dV, \quad (35)$$

The total angular momentum J is given by (see Problem 6 of [18])

$$J = - \int T_{\alpha\beta} n^\alpha \chi^\beta dV = \int J_{\hat{\varphi}} r \sin \theta dV, \quad (36)$$

where χ^α is the axial Killing vector of the spacetime. The rotational kinetic energy for a uniformly rotating star is $T = \frac{1}{2}\Omega J$. The gravitational potential energy is

$$W = M_p + T - M_g, \quad (37)$$

where M_p is the proper mass of the star defined by

$$M_p = \int [-n_\alpha (eu^\alpha)] dV = \int \Gamma e dV. \quad (38)$$

Note that W is defined to be positive.

Furthermore, two relativistic virial identities (the so-called GRV2 and GRV3) have been proved to be useful for checking the consistency and accuracy of numerical solutions of rotating relativistic star models. The three-dimensional virial identity GRV3 [19] is a relativistic generalisation of the Newtonian virial identity, valid for any stationary and asymptotically flat spacetime. The two-dimensional virial identity GRV2 [20] is valid for any asymptotically flat spacetime (without any symmetry assumption). The two virial identities are integral relations between the matter and metric fields (see [19, 20] for expressions). In practice, we define the quantities $GRV2 := |1 - \lambda_2|$ and $GRV3 := |1 - \lambda_3|$ as the error indicators for the virial identities, where λ_2 and λ_3 are defined via the integral relations, such that exact solutions of the Einstein equations satisfy $GRV2 = GRV3 = 0$ (see [21]). Note that these identities are not imposed during the numerical calculation, and hence are useful indicators for checking the accuracy of numerical results.

3. Numerical results

3.1. Numerical procedure

To calculate stationary axisymmetric rotating stars within the Dirac gauge and maximal slicing, we solve the nonlinear elliptic equations described in Sec. 2.3 iteratively by means of multi-domain spectral methods [22, 23] in spherical coordinates. The code is constructed upon the LORENE C++ library [16]. We use three spherical numerical domains to cover the whole hypersurface Σ_t . Specifically, we use one domain to cover the whole star and one domain for the space around the star (typically to about twice the stellar radius). The last domain covers the space out to spatial infinity by means of a compactification $u = 1/r$ [14].

In each domain, we use N_θ collocation points in the polar direction and $N_\varphi = 1$ point in the azimuthal direction for the spectral method. For the radial direction, we

can choose to have different numbers of collocation points in different domains. In Sec. 3.3, we use the notation $N_r = (N_{r1}, N_{r2}, N_{r3})$, where N_{r1} denotes the number of points in the first domain etc, to specify the grid structure in the radial direction.

The numerical iteration procedure is briefly described here. For a given equation of state, we choose Ω and the central value of the log-enthalpy H (see Eq. (16)) as the physical parameters that specify the rotating star model. First we start with an initial guess by setting all the metric quantities to their flat spacetime values, together with a spherically symmetric distribution for the matter sources. The iteration procedure begins by solving Eqs. (19) and (26) respectively for the corresponding lapse and shift. Thus, we obtain the only nonzero component of the 3-velocity $v^\phi = (\Omega r \sin \theta + \beta^\phi)/N$ (see Eq. (12)), and hence the Lorentz factor Γ . Next we use the first integral of motion (Eq. (15)) to obtain H . Finally, we solve Eqs. (24) and (28) respectively for Q and h^{ij} . The iteration procedure continues until the relative difference in H throughout the whole star between two consecutive steps is smaller than some prescribed value.

The resolutions of the scalar Poisson equations for N and Q , and the vectorial elliptic equation for β^i have been described in details in [24]. The technique for solving the tensorial Poisson equation (28) is described in Appendix A.

3.2. Equation of state

In Sec. 3.3, we present various tests that have been done to validate our numerical code. For this purpose, we use a polytropic EOS in the following form to construct rotating neutron star models:

$$P = \kappa n^\gamma, \quad (39)$$

where κ and γ are constants. The number density n is related to the energy density e by

$$e = m_B n + \frac{\kappa}{\gamma - 1} n^\gamma, \quad (40)$$

where the baryon mass $m_B = 1.66 \times 10^{-24}$ g. In particular, we take $\gamma = 2$ and $\kappa = 0.03 \rho_{\text{nuc}} c^2 / n_{\text{nuc}}^2$, where $\rho_{\text{nuc}} = 1.66 \times 10^{14}$ g cm $^{-3}$ and $n_{\text{nuc}} = 0.1$ fm $^{-3}$. For this EOS, the log-enthalpy is given analytically by

$$H = \ln \left[1 + \frac{\kappa \gamma}{m_B (\gamma - 1)} n^{\gamma-1} \right]. \quad (41)$$

We also use the simplest MIT bag model EOS, with noninteracting massless quarks, to construct rapidly rotating strange stars. The EOS is given in the following form (see, e.g., [15])

$$\begin{aligned} P &= \frac{1}{3} a n^{4/3} - B, \\ e &= a n^{4/3} + B, \end{aligned} \quad (42)$$

where B is the MIT bag constant and the parameter $a = 9\pi^{2/3} \hbar c / 4 = 952.371$ MeV fm. We choose $B = 60$ MeV fm $^{-3}$ in this work. The stellar surface is characterised by the properties of strange matter at zero pressure: the number density $n_0 = 0.28665$ fm $^{-3}$ and the mass density $\rho_0 = 4.2785 \times 10^{14}$ g cm $^{-3}$. The log-enthalpy is related to n simply by $H = \ln(n/n_0)^{1/3}$. The MIT bag model EOS is useful to test our numerical code in the highly relativistic regime, since strange stars can reach higher compactness ratios and rotation rates than ordinary neutron stars.

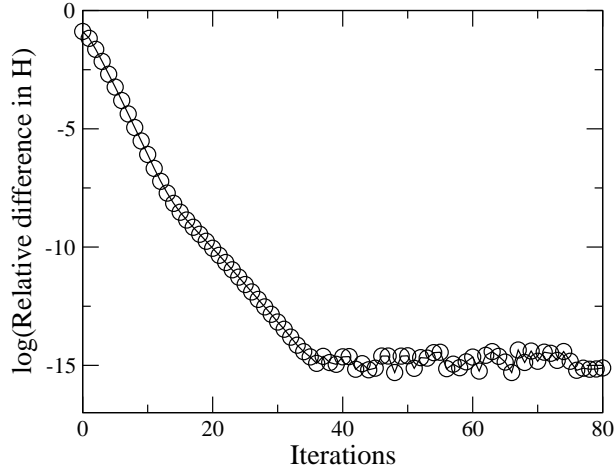


Figure 1. Convergence towards zero of the relative difference in H throughout the star between two consecutive steps for a non-rotating polytropic star model (see text).

3.3. Tests of the numerical code

To test our numerical code, we start with a non-rotating star modelled by the polytropic EOS described in Sec. 3.2. The central value of the log-enthalpy is $H_0 = 0.2308$ (or equivalently the energy density $e_0 = 4.889\rho_{\text{nuc}}c^2$) and the baryon mass of the star is $M_b = 1.6M_\odot$. The star has a gravitational mass $M_g = 1.4866M_\odot$ and a compactness ratio $M_g/R = 0.147$, where R is the circumferential radius. In the numerical calculations, we use a parameter ϵ_H (typically set to be 10^{-10} or smaller) to control the iteration procedure and the precision of the numerical models: the iteration (see Sec. 3.1) is stopped if the relative difference in H throughout the whole star between two consecutive steps is smaller than ϵ_H . In Fig. 1, we show the convergence of the relative difference in H towards zero with the number of iterations using radial collocation points $N_r = (33, 33, 17)$. We see that a precision of 10^{-15} is achieved for the numerical result within 40 iteration steps. After that, the accuracy is limited by the round-off errors. The solution also satisfies the virial identities to the level of 10^{-15} .

Next, we test the convergence property of the numerical code with respect to increasing number of radial collocation points using the same model. In particular, we vary the number of points in the first numerical domain (i.e., inside the star), while keeping the points in the other two domains fixed to $N_{r2} = 33$ and $N_{r3} = 17$, and we choose $\epsilon_H = 10^{-15}$ in this test. In Fig. 2, we plot $\log(GRV2)$ and $\log(GRV3)$ together against the number of points N_{r1} in the first domain. It is seen clearly that both $GRV2$ and $GRV3$ converge exponentially towards zero with the number of points, as expected for spectral methods. The accuracy is limited by the round-off errors for $N_{r1} > 30$.

Starting from the above non-rotating polytropic model, we then construct a sequence of increasing uniformly rotating configurations at fixed baryon mass $M_b = 1.6M_\odot$, up to the mass-shedding limit. The accuracy of the numerical models are estimated by comparing the results to those obtained by a separated code LORENE-

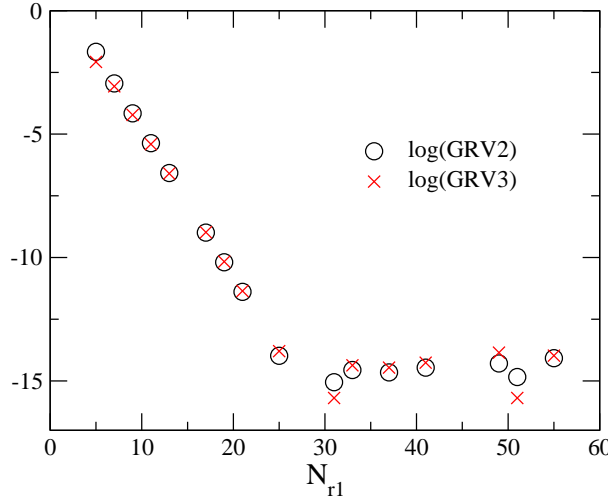


Figure 2. Convergence towards zero of *GRV2* and *GRV3* with the number of collocation points N_{r1} inside the star for the same model as shown in Fig. 1.

rotstar [14, 15], which uses the so-called quasi-isotropic gauge to construct rotating relativistic stars. LORENE-rotstar is a well-established code which has been tested extensively and compared with a few different numerical codes [21]. A comparison of some of the gauge invariant quantities for the sequence between our code and LORENE-rotstar is given in Table 1. The parameters used to obtain the numerical results are $N_r = (33, 17, 17)$, $N_\theta = 17$, and $\epsilon_H = 10^{-10}$ for both codes. In the table, for each value of the rotation frequency f , we display the results obtained from our numerical code based on the Dirac gauge in the first row. Below this are the results obtained from LORENE-rotstar. Table 1 shows that the two sets of results agree to high accuracy. In particular, the overall discrepancy between the two different codes is consistent with the errors in the virial identities, which increase with the rotation frequency. Note that the errors in the virial identities for the non-rotating configuration listed in the table is about 10^{-9} instead of 10^{-15} as shown in Fig. 2. This is due to our choice of using $\epsilon_H = 10^{-10}$ in this test.

We note, however, that the numerical error no longer decreases exponentially with the number of grid points as in the non-rotating case (see Fig 2), but as a power-law, due to the discontinuities in the derivative of the matter fields at the stellar surface. The non-rotating model is free from any such phenomenon because the stellar surface is at the boundary between two spherical numerical domains. For rotating models, because of the flattening of the stars, the stellar surface no longer coincides with the boundary of the domains, and hence the spectral method loses its exponential-convergence property. Such difficulty associated with rotating stars can be handled by the adaptation of the numerical domains to the stellar surface as developed in [22]. We plan to improve our numerical code by implementing this surface-adaptation technique in the near future[‡]. Nevertheless, even without a surface-adaptation technique, Table 1 shows that both numerical codes still agree to high accuracy and achieve a precision of

[‡] Such numerical technique is already available in LORENE-rotstar as described in [15]. However, in order to compare to our numerical code, the results obtained from LORENE-rotstar as listed in Table 1 are based on fixed spherical numerical domains.

Table 1. Comparison between our numerical code based on the Dirac gauge and a well-established code LORENE-rotstar, which uses a quasi-isotropic gauge for the coordinates, for a sequence of $\gamma = 2$ polytropic neutron star models with fixed baryon mass $M_b = 1.6M_\odot$. Listed are the rotation frequency f , gravitational mass M_g , total angular momentum parameter J/M_g^2 , ratio of the rotational kinetic energy to the potential energy T/W , equatorial circumferential radius R_{eq} , and errors indicators in the virial identities *GRV2* and *GRV3*.

f (Hz)	$M_g(M_\odot)$	J/M_g^2	T/W	R_{eq} (km)	<i>GRV2</i>	<i>GRV3</i>
0	1.486610961	0	0	14.91222928	7e-9	2e-9
	1.486610965	0	0	14.91222929	9e-9	1e-9
100	1.486837016	0.066036124	0.00107222950	14.9609161	3e-9	3e-8
	1.486837013	0.066036126	0.00107222954	14.9609165	3e-8	5e-8
200	1.487539907	0.13421663	0.004395974	15.113935	2e-7	5e-7
	1.487539902	0.13421665	0.004395975	15.113937	3e-7	7e-7
300	1.4888008	0.2072617	0.010340091	15.395905	3e-7	6e-7
	1.4888007	0.2072618	0.010340095	15.395908	2e-8	6e-7
400	1.49080352	0.289551	0.01973704	15.865576	1e-6	3e-6
	1.49080359	0.289550	0.01973701	15.865574	7e-7	4e-6
500	1.493991	0.390430	0.0345952	16.67896	4e-6	8e-6
	1.493990	0.390432	0.0345954	16.67900	6e-6	1e-5
550	1.4964095	0.455303	0.0457202	17.35894	2e-5	2e-5
	1.4964092	0.455307	0.0457206	17.35898	1e-5	2e-5
600	1.500054	0.54397	0.062368	18.5382	5e-6	2e-6
	1.500055	0.54398	0.062369	18.5383	3e-6	3e-6
$640 \approx f_k$	1.506928	0.695855	0.0929183	22.1467	2e-5	5e-5
	1.506929	0.695857	0.0929188	22.1469	1e-5	6e-5

10^{-5} for a configuration rotating near the mass-shedding limit (i.e., the $f = 640 \approx f_k$ Hz configuration in Table 1, where f_k is the Kepler frequency). To visualise the gravitational field generated by a rotating star, we plot in Figs. 3-6 the non-vanishing components for the metric field h^{ij} (namely, $h^{\hat{r}\hat{r}}$, $h^{\hat{r}\hat{\theta}}$, $h^{\hat{\theta}\hat{\theta}}$, and $h^{\hat{\varphi}\hat{\varphi}}$) for the rotating star model with $f = 640$ Hz. In these figures, we show the iso-contours of the fields in the meridional plane, where solid (dashed) lines indicate positive (negative) values of the fields. The thick solid lines represent the stellar surface. Finally, the dot-dashed circles represent the boundary between the first two spherical numerical domains. The figures show clearly that the gravitational field is dominated by the quadrupole moment.

To further calibrate our numerical code against LORENE-rotstar, we now compare the two codes using a very relativistic and rapidly rotating strange star model. The matter is described by the MIT bag model as described in Sec. 3.2. This configuration, shown in Fig. 7, has a baryon mass $M_b = 2.2M_\odot$ and compactness ratio $M_g/R_{eq} = 0.204$ (with the gravitational mass $M_g = 1.719M_\odot$ and the circumferential equatorial radius $R_{eq} = 12.425$ km). The rotation frequency is $f = 1000$ Hz. In Table 2, we show the values of various physical quantities obtained from both numerical codes, together with the relative difference between them. As in the case of the polytropic EOS model, the discrepancy of the two numerical codes is consistent with the errors in *GRV2* and *GRV3*. Note also that, even with a strong density discontinuity at the strange star surface, our numerical model still achieves a precision of 10^{-3} .

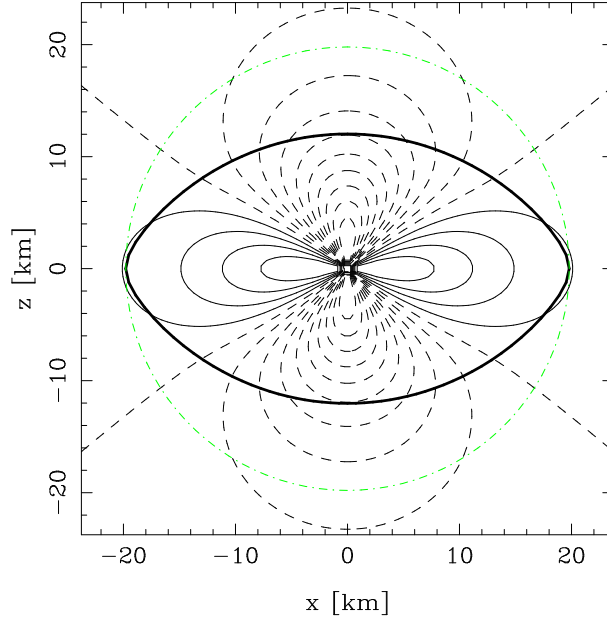


Figure 3. Iso-contours of the metric component $h^{\hat{r}\hat{r}}$ in the meridional plane for the $f = 640$ Hz rotating polytropic model given in Table 1. The solid (dashed) lines indicate positive (negative) values of the field. The thick solid line represents the stellar surface. The dot-dashed circle is the boundary between the first two spherical numerical domains.

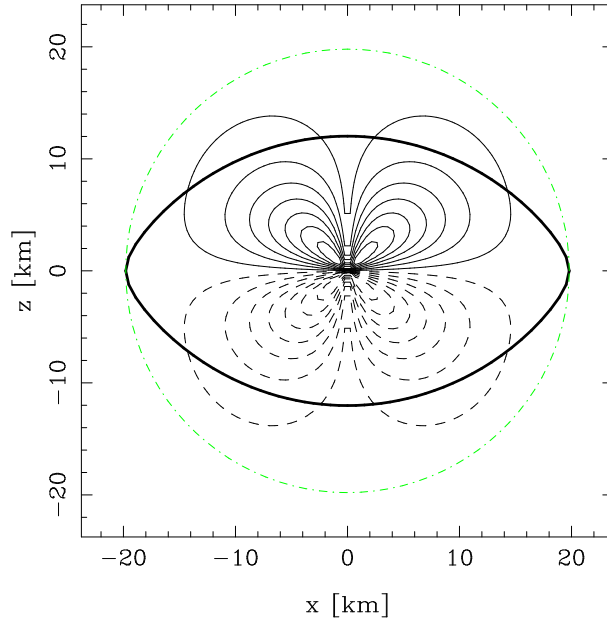


Figure 4. Same as Fig. 3 but for the component $h^{\hat{r}\hat{\theta}}$.

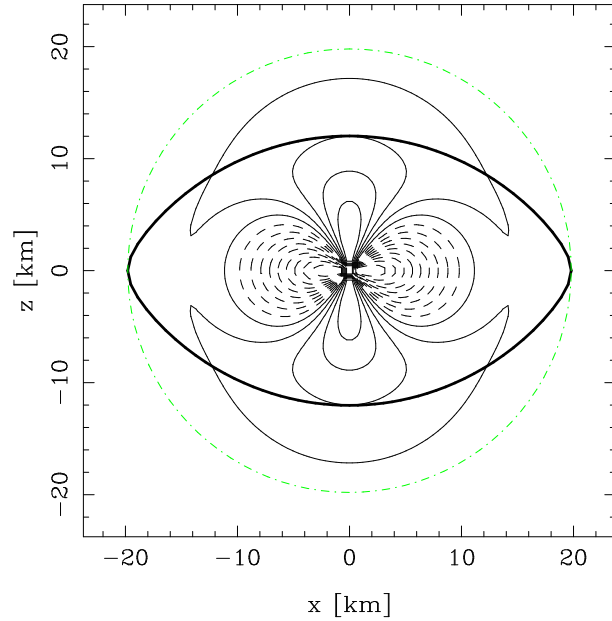


Figure 5. Same as Fig. 3 but for the component $h^{\hat{\theta}\hat{\theta}}$.

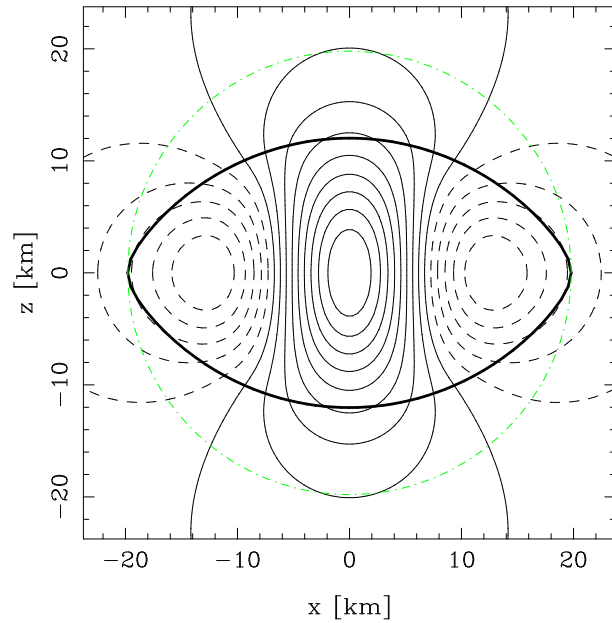


Figure 6. Same as Fig. 6 but for the component $h^{\hat{\phi}\hat{\phi}}$.

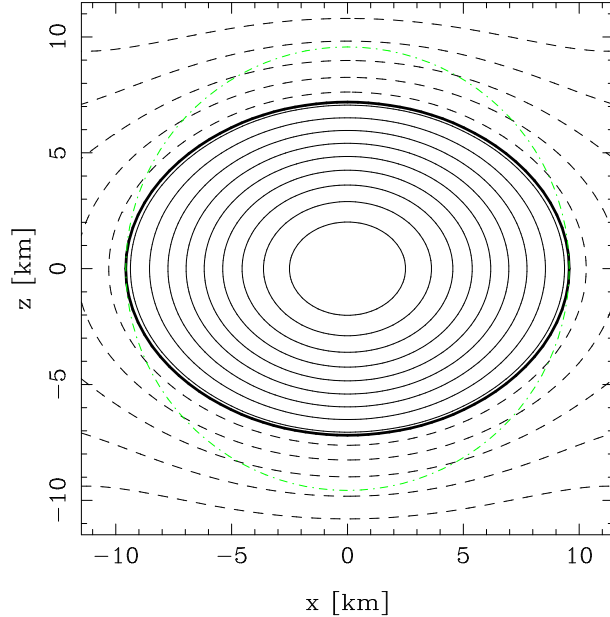


Figure 7. Meridional plane cross section of a rapidly rotating strange star. The star has a baryon mass $M_b = 2.3M_\odot$, gravitational mass $M_g = 1.787M_\odot$, and rotation frequency $f = 1000$ Hz. The lines are iso-contours of the log-enthalpy H . The thick solid line represents the stellar surface. Outside the star, H is defined by the first integral of motion Eq. (15).

Table 2. Comparison between our numerical code (LORENE-rotstar_dirac) and LORENE-rotstar for a rapidly rotating strange star model. The star has a baryon mass $M_b = 2.2M_\odot$, gravitational mass $M_g = 1.719M_\odot$, and rotation frequency $f = 1000$ Hz.

	rotstar_dirac	rotstar	rel. diff.
$M_g(M_\odot)$	1.7194	1.7198	2e-4
J/M_g^2	0.5940	0.5945	8e-4
T/W	0.0888	0.0890	2e-3
R_{eq} (km)	12.425	12.433	7e-4
$GRV2$	7e-4	2e-4	
$GRV3$	1e-3	6e-4	

4. Conclusion

In this paper we have developed a computer code (LORENE-rotstar_dirac) to construct relativistic rotating stars within the framework of a new constrained-evolution formulation of the $3 + 1$ Einstein equations based on the Dirac gauge and maximal slicing [13]. As the Dirac gauge fixes the spatial coordinates on each time slices, including the initial one, this formulation can be used to compute stationary solutions of the Einstein equations simply by setting the time derivative terms in various equations to zeros. The system reduces to two scalar elliptic equations for the lapse function N and conformal factor Ψ (equivalently for $Q := \Psi^2 N$), a vectorial elliptic equation for the shift vector β^i , and a tensorial elliptic equation for a tensor field h^{ij} . We couple this system of equations to the first integral of motion for the

matter, and solve the equations iteratively using multi-domain spectral method.

We have demonstrated that this formulation can be used to compute stationary rotating equilibrium configurations to high accuracy. In particular, we used the polytropic EOS and MIT bag model to calculate rotating neutron star and strange star models respectively. We compared our code to a well-established code LORENE-rotstar, which uses a quasi-isotropic gauge to fix the coordinates, and found that the global quantities of the numerical models obtained from the two codes agree to high accuracy. The discrepancy between the two codes is consistent to the errors in the virial identities.

Finally, we remark that the proposed constrained-evolution scheme [13] is particular well suited to the conformally-flat relativistic hydrodynamics code, with a metric solver based on spectral methods and spherical coordinates, developed by Dimmelmeier *et al.* in the so-called *Mariage des Maillages* (MDM) project [25]. The numerical code that we described in this paper can be used to generate rotating-star initial data for hydrodynamics simulations in full general relativity within the new constrained-evolution scheme [13] for the MDM project.

Acknowledgments

We thank Silvano Bonazzola, Éric Gourgoulhon and Philippe Grandclément for helpful discussions and hints for this work. L.M.L is supported by a Croucher Foundation fellowship.

Appendix A. Resolution of the Poisson equations for h^{ij}

Here we describe the numerical strategy used to solve the tensorial Poisson equation (28), imposing that the solution h^{ij} verify the gauge condition (23) and be such that the conformal metric has a unitary determinant:

$$\det(\hat{\gamma}^{\hat{i}\hat{j}} = f^{\hat{i}\hat{j}} + h^{\hat{i}\hat{j}}) = 1. \quad (\text{A.1})$$

Note that this relation follows directly from the definition of the conformal factor in the proposed constrained scheme (see Eqs. (17) and (18)), together with the condition $\det f_{\hat{i}\hat{j}} = 1$ in the orthonormal basis (\mathbf{e}_i) (see Sec. 2.4). In Ref. [13], one would solve two (scalar) Poisson equations: for $h^{\hat{r}\hat{r}}$ and the potential μ (see Eq. (A.8)); the other four components are deduced from the three gauge conditions and the non-linear relation (A.1) through an iteration. The drawback of this method is that some components of h^{ij} are calculated as second radial derivatives of $h^{\hat{r}\hat{r}}$ and μ . Since the source of Eq. (28) contains second-order radial derivatives of h^{ij} , one needs to calculate fourth-order radial derivatives of $h^{\hat{r}\hat{r}}$ and μ , which are solutions of scalar-like Poisson equations with matter terms on the RHS. In the case of neutron stars, it is quite often that radial density profiles have a discontinuous derivative at the surface of the star. Therefore, $h^{\hat{r}\hat{r}}$ and μ admit discontinuous third-order radial derivatives and their fourth-order derivatives cannot be represented at all by means of spectral methods. A solution could be to use adaptive mapping: the boundary between two spectral domains coincides with the (non-spherical) surface of the star (see [22]). Still, the evaluation of a fourth-order radial derivative introduces too much numerical noise, even using spectral methods. We have therefore chosen to use a different approach, detailed hereafter.

Instead of using directly all the spherical components of the tensor h^{ij} , we use only the $\hat{r}\hat{r}$ - component, the trace $h = f_{ij}h^{ij}$ and the four potentials η , μ , W and X defined as follow, in the orthonormal basis (e_i):

$$h^{\hat{r}\hat{\theta}} = \frac{1}{r} \left(\frac{\partial \eta}{\partial \theta} - \frac{1}{\sin \theta} \frac{\partial \mu}{\partial \varphi} \right), \quad (\text{A.2})$$

$$h^{\hat{r}\hat{\varphi}} = \frac{1}{r} \left(\frac{1}{\sin \theta} \frac{\partial \eta}{\partial \varphi} + \frac{\partial \mu}{\partial \theta} \right), \quad (\text{A.3})$$

and

$$P = \frac{\partial^2 W}{\partial \theta^2} - \frac{1}{\tan \theta} \frac{\partial W}{\partial \theta} - \frac{1}{\sin^2 \theta} \frac{\partial^2 W}{\partial \varphi^2} - 2 \frac{\partial}{\partial \theta} \left(\frac{1}{\sin \theta} \frac{\partial X}{\partial \varphi} \right), \quad (\text{A.4})$$

$$h^{\hat{\theta}\hat{\varphi}} = \frac{\partial^2 X}{\partial \theta^2} - \frac{1}{\tan \theta} \frac{\partial X}{\partial \theta} - \frac{1}{\sin^2 \theta} \frac{\partial^2 X}{\partial \varphi^2} + 2 \frac{\partial}{\partial \theta} \left(\frac{1}{\sin \theta} \frac{\partial W}{\partial \varphi} \right); \quad (\text{A.5})$$

with $P = (h^{\hat{\theta}\hat{\theta}} - h^{\hat{\varphi}\hat{\varphi}})/2$. These equations can be inverted to compute the potentials in terms of the angular part of the Laplace operator

$$\Delta_{\theta\varphi} = \frac{\partial^2}{\partial \theta^2} + \frac{1}{\tan \theta} \frac{\partial}{\partial \theta} + \frac{1}{\sin^2 \theta} \frac{\partial^2}{\partial \varphi^2}, \quad (\text{A.6})$$

giving

$$\Delta_{\theta\varphi} \eta = r \left(\frac{\partial h^{\hat{r}\hat{\theta}}}{\partial \theta} + \frac{h^{\hat{r}\hat{\theta}}}{\tan \theta} + \frac{1}{\sin \theta} \frac{\partial h^{\hat{r}\hat{\varphi}}}{\partial \varphi} \right), \quad (\text{A.7})$$

$$\Delta_{\theta\varphi} \mu = r \left(\frac{\partial h^{\hat{r}\hat{\varphi}}}{\partial \theta} + \frac{h^{\hat{r}\hat{\varphi}}}{\tan \theta} - \frac{1}{\sin \theta} \frac{\partial h^{\hat{r}\hat{\theta}}}{\partial \varphi} \right), \quad (\text{A.8})$$

$$\begin{aligned} \Delta_{\theta\varphi} (\Delta_{\theta\varphi} + 2) W = & \frac{\partial^2 P}{\partial \theta^2} + \frac{3}{\tan \theta} \frac{\partial P}{\partial \theta} - \frac{1}{\sin^2 \theta} \frac{\partial^2 P}{\partial \varphi^2} - 2P \\ & + \frac{2}{\sin \theta} \frac{\partial}{\partial \varphi} \left(\frac{\partial h^{\hat{\theta}\hat{\varphi}}}{\partial \theta} + \frac{h^{\hat{\theta}\hat{\varphi}}}{\tan \theta} \right), \end{aligned} \quad (\text{A.9})$$

$$\begin{aligned} \Delta_{\theta\varphi} (\Delta_{\theta\varphi} + 2) X = & \frac{\partial^2 h^{\hat{\theta}\hat{\varphi}}}{\partial \theta^2} + \frac{3}{\tan \theta} \frac{\partial h^{\hat{\theta}\hat{\varphi}}}{\partial \theta} - \frac{1}{\sin^2 \theta} \frac{\partial^2 h^{\hat{\theta}\hat{\varphi}}}{\partial \varphi^2} - 2h^{\hat{\theta}\hat{\varphi}} \\ & - \frac{2}{\sin \theta} \frac{\partial}{\partial \varphi} \left(\frac{\partial P}{\partial \theta} + \frac{P}{\tan \theta} \right). \end{aligned} \quad (\text{A.10})$$

These quantities η, μ, W, X are interesting for, at least, two reasons: first they can be expanded onto a basis of scalar spherical harmonics $Y_\ell^m(\theta, \varphi)$, which are often used in the framework of spectral methods, for they are eigenfunctions of the angular Laplace operator (A.6). Furthermore, the three gauge conditions (23) can be reformulated in terms of these potentials:

$$\frac{\partial h^{\hat{r}\hat{r}}}{\partial r} + \frac{3h^{\hat{r}\hat{r}}}{r} + \frac{1}{r^2} \Delta_{\theta\varphi} \eta - \frac{h}{r} = 0, \quad (\text{A.11})$$

$$\frac{\partial \eta}{\partial r} + \frac{2\eta}{r} + (\Delta_{\theta\varphi} + 2) W + \frac{1}{2} (h - h^{\hat{r}\hat{r}}) = 0, \quad (\text{A.12})$$

$$\frac{\partial \mu}{\partial r} + \frac{2\mu}{r} + (\Delta_{\theta\varphi} + 2) X = 0. \quad (\text{A.13})$$

When decomposing the fields on a basis of spherical harmonics, these relations reduce to a system of ordinary differential equations with respect to r , which is solved by spectral methods in a similar way to the Poisson equation [24].

The numerical algorithm is then:

- (i) transform the source term of Eq. (28) to the Cartesian basis,
- (ii) solve the resulting six decoupled scalar Poisson equations for h^{ij} ,
- (iii) transform h^{ij} back to the spherical basis and compute the potentials W and X ,
- (iv) do an iteration on h , first solving the system (A.11)-(A.13) with h , W and X as sources and then calculating the new value of h from the non-linear equation (A.1).

Since the system is overdetermined (four additional relations to satisfy), the integrability condition is that the source of the tensor Poisson equation (28) be divergence-free. We do not impose this condition during the main iteration of the code, since this is not true for intermediate solutions of the metric and matter fields. We only check that this is verified, up to the accuracy of the code, at the end of the iteration, and we have found that this was true at the error level given by the virial identities (see Sec. 2.4). The potentials W and X have been chosen among the six degrees of freedom of h^{ij} because none of their radial derivatives appear in the gauge conditions (A.11)-(A.13), hence, we do not calculate any radial derivative of these quantities to get the other components of h^{ij} . Another reason for this choice is that, when considering a more general case of dynamically evolving spacetime, these two potentials are asymptotically related to the two gravitational wave polarisation modes: $P \rightarrow h_+$ and $h^{\theta\varphi} \rightarrow h_\times$ in our asymptotically transverse-traceless gauge[§]. Note that in our case of stationary and axisymmetric spacetime, we have $\mu = X = 0$, which simplifies the resolution.

- [1] York J W 1979 *Sources of Gravitational Radiation* ed L Smarr (Cambridge: Cambridge University Press) p 83
- [2] Baumgarte T W and Shapiro S L 2003 *Phys. Rep.* **376** 41
- [3] Calabrese G, Lehner L, Tiglio M 2002 *Phys. Rev. D* **65** 104031
- [4] Lindblom L, Scheel M A, Kidder L E, Pfeiffer H P, Shoemaker D, Teukolsky S A 2004 *Phys. Rev. D* **69** 124025
- [5] Kidder L E, Lindblom L, Scheel M A, Buchman L T, Pfeiffer H P 2005 *Phys. Rev. D* **71** 064020
- [6] Holst M, Lindblom L, Owen R, Pfeiffer H P, Scheel M A, and Kidder L E 2004 *Phys. Rev. D* **70** 084017
- [7] Tiglio M, Lehner L, Neilsen D 2004 *Phys. Rev. D* **70** 104018
- [8] Gentle A P, George N D, Kheyfets A, and Miller W A 2004 *Class. Quantum Grav.* **21** 83
- [9] Stark R F and Piran T 1985 *Phys. Rev. Lett.* **55** 891
- [10] Choptuik M W 1993 *Phys. Rev. Lett.* **70** 9
- [11] Abrahams A M, Cook G B, Shapiro S L, and Teukolsky S A 1994 *Phys. Rev. D* **49** 5153
- [12] Choptuik M W, Hirschmann E W, Liebling S L, and Pretorius F 2003 *Class. Quantum Grav.* **20** 1857
- [13] Bonazzola S, Gourgoulhon E, Grandclément P, and Novak J 2004 *Phys. Rev. D* **70** 104007
- [14] Bonazzola S, Gourgoulhon E, Salgado M, and Marck J A 1993 *Astron. Astrophys.* **278** 421
- [15] Gourgoulhon E, Haensel P, Livine R, Paluch E, Bonazzola S, and Marck J A 1999 *Astron. Astrophys.* **349** 851
- [16] <http://www.lorene.obspm.fr/>
- [17] Carter B 1970 *Comm. Math. Phys.* **17** 233
- [18] Wald R M 1984 *General Relativity* (Chicago: The University of Chicago Press)
- [19] Gourgoulhon E and Bonazzola S 1994 *Class. Quantum Grav.* **11** 443
- [20] Bonazzola S and Gourgoulhon E 1994 *Class. Quantum Grav.* **11** 1775
- [21] Nozawa T, Stergioulas N, Gourgoulhon E, and Eriguchi Y 1998 *Astron. Astrophys. Suppl. Ser.* **132** 431
- [22] Bonazzola S, Gourgoulhon E, and Marck J A 1998 *Phys. Rev. D* **58** 104020
- [23] Bonazzola S, Gourgoulhon E, and Marck J A 1999 *J. Comput. Appl. Math.* **109** 433
- [24] Grandclément P, Bonazzola S, Gourgoulhon E, Marck J A 2001 *J. Comput. Phys.* **170** 231
- [25] Dimmelmeier H, Novak J, Font J A, Ibáñez J M, and Müller E 2005 *Phys. Rev. D* **71** 064023

[§] The condition (A.1) implies that $h = 0$ to the linear order